Mechanisms of mutagenesis *in vivo* due to imbalanced dNTP pools

Dinesh Kumar[1], Amy L. Abdulovic[2], Jörgen Viberg[1], Anna Karin Nilsson[1], Thomas A. Kunkel[2] and Andrei Chabes[1,3,*]

[1]Department of Medical Biochemistry and Biophysics, Umeå University, SE-901 87 Umeå, Sweden,
[2]Laboratory of Molecular Genetics and Laboratory of Structural Biology, National Institutes of Environmental Health Sciences, National Institutes of Health, DHHS, Research Triangle Park, NC 27709, USA and
[3]Laboratory for Molecular Infection Medicine Sweden (MIMS), Umeå University, SE 90187 Umeå, Sweden

ABSTRACT

The mechanisms by which imbalanced dNTPs induce mutations have been well characterized within a test tube, but not *in vivo*. We have examined mechanisms by which dNTP imbalances induce genome instability in strains of *Saccharomyces cerevisiae* with different amino acid substitutions in Rnr1, the large subunit of ribonucleotide reductase. These strains have different dNTP imbalances that correlate with elevated *CAN1* mutation rates, with both substitution and insertion–deletion rates increasing by 10- to 300-fold. The locations of the mutations in a strain with elevated dTTP and dCTP are completely different from those in a strain with elevated dATP and dGTP. Thus, imbalanced dNTPs reduce genome stability in a manner that is highly dependent on the nature and degree of the imbalance. Mutagenesis is enhanced despite the availability of proofreading and mismatch repair. The mutations can be explained by imbalanced dNTP-induced increases in misinsertion, strand misalignment and mismatch extension at the expense of proofreading. This implies that the relative dNTP concentrations measured in extracts are truly available to a replication fork *in vivo*. An interesting mutational strand bias is observed in one *rnr1* strain, suggesting that the S-phase checkpoint selectively prevents replication errors during leading strand replication.

INTRODUCTION

The four deoxyribonucleoside triphosphates, dATP, dTTP, dGTP and dCTP, are essential precursors for the DNA synthesis, which is required for replication, recombination and repair. Because these DNA transactions are needed to maintain genome stability, perturbations in the absolute and relative concentrations of the four dNTPs increase mutation rates by reducing the fidelity of DNA synthesis (1). Changes in dNTPs concentration are mutagenic and may occur due to mutations in enzymes involved in dNTP metabolism or changes in the environment. The mutational mechanisms induced by imbalanced dNTP pools within cells have not been extensively investigated. *In vitro* studies performed with purified DNA polymerases have revealed several mechanisms by which dNTP perturbations reduce fidelity [reviewed in (2)]. One mechanism predicts that imbalanced dNTP pools increase the probability that a DNA polymerase will misinsert an incorrect dNTP [reviewed in (3)]. For example, an abnormally high ratio of dTTP as compared to dGTP can promote misinsertion (MI) of dTTP opposite a template C (Figure 1, top left). Additional studies *in vitro* indicate that imbalanced dNTP concentrations can also increase the rate of formation of insertion–deletion (indel) errors during DNA synthesis (4,5). For instance, when the ratio of the correct dNTP to the incorrect dNTP needed for synthesis within a mononucleotide run strongly favors the incorrect dNTP, the probability of DNA strand misalignment (MA) (Figure 1, top right) is increased, thereby increasing indel error rates. Alternatively, a dNTP imbalance may induce an MI that, in the appropriate sequence context, can result in primer relocation [(PR), Figure 1, second pathway from
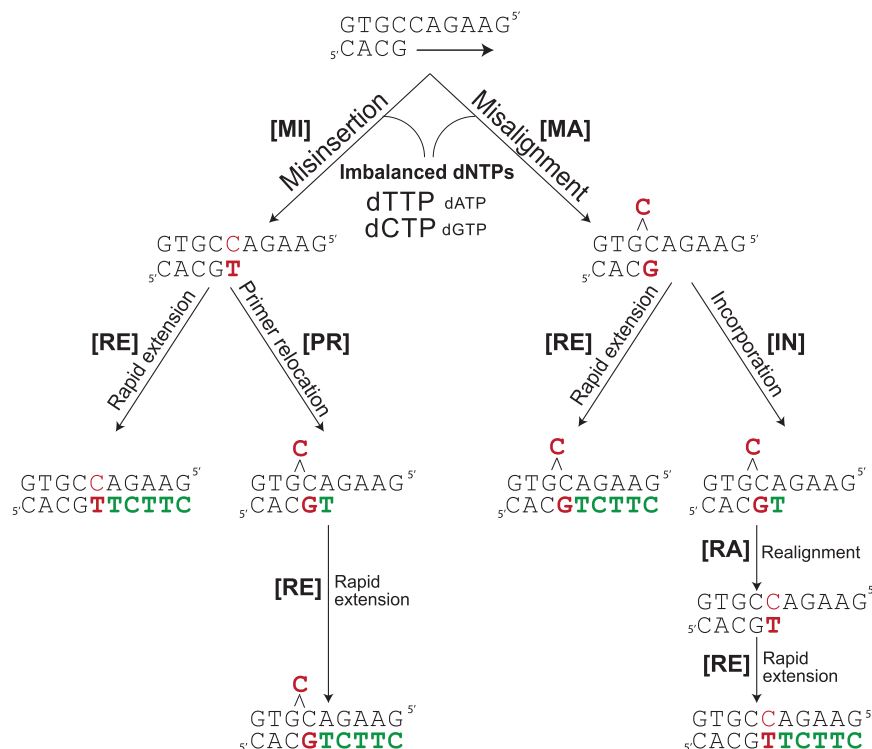
Figure 1. Models for substitutions and deletions resulting from imbalanced dNTP pools. MI: misinsertion; MA: misalignment; PR: primer relocation; RE: rapid extension; IN: incorporation; RA: realignment. Red characters represent the mutational event and green characters represent bases where the dNTP is at an excessively high concentration.

left] to create an indel intermediate with one or more correct terminal base pairs. Another possibility supported by evidence *in vitro* (5–10) is MA followed by correct incorporation (IN), then realignment (RA), thereby creating a base–base mismatch that was initiated by MA (Figure 1, rightmost pathway). Finally, *in vitro* studies show that the probability that mismatches will eventually result in substitutions or indels are increased if the nucleotides to be incorporated immediately following the mismatch (colored green in Figure 1) are present at high enough concentrations to promote rapid extension (RE) from the mismatch prior to proofreading and/or RA [reviewed in (3,7)].

The goal of the present study is to determine the extent to which the concepts outlined in Figure 1 may explain the specificity of mutagenesis observed *in vivo* when dNTP pools are perturbed. In previous studies, mutations induced by dNTP pool imbalances were analyzed in phage T4 (*rII* and thymidine kinase genes), *Escherichia coli* (*lacI* gene), *Saccharomyces cerevisiae* (*SUP4-o* gene), mouse (integrated bacterial *gpt* gene), Chinese hamster (*aprt* gene) and human (*HPRT* gene) cells (11–22). The majority of the mutations produced by dNTP pool imbalances were found to be single base pair events dominated by substitutions, whereas indels were recovered less frequently and not in each investigation. Some of these studies suggested that dNTP pool imbalances promote mutagenesis by suppressing proofreading activity of DNA polymerases (2). In this study, we took advantage of recent structure–function studies that have advanced our understanding of how dNTP pools are regulated by ribonucleotide reductase (RNR) (23). RNR is responsible for catalyzing the rate-limiting step in the synthesis of all four dNTPs and is comprised of multiple subunits. Yeast RNR is highly regulated on many levels: at the G1/S boundary and in response to DNA damage, RNR genes are transcriptionally upregulated (24–27), the levels of the RNR inhibitor Sml1 are post-transcriptionally reduced (28) and the small subunit Rnr2/Rnr4 proteins are re-distributed to the cytoplasm, where the large subunit Rnr1/Rnr3 proteins are localized (29–31). Additionally, the activity of RNR is controlled allosterically (32). The large subunit contains an allosteric specificity site responsible for controlling the balance of the four dNTPs. The specificity site influences the specific ribonucleoside diphosphate reduction reaction within the catalytic site, which is also present in the large subunit (33).

In this study, we utilized yeast strains with single amino acid substitutions in loop 2 of Rnr1 (23). Loop 2 is highly conserved throughout the evolutionary ladder from yeast through humans (34–36). The residues of loop 2 are important for the connection between the specificity site and the catalytic site (34,36). Specifically, three yeast strains were created that encode a different single amino acid change in one of two conserved residues in loop 2, tyrosine 285 (Y285) or glutamine 288 (Q288). As previously reported, strains with a change at Y285 have no

noticeable proliferation defects, whereas strains with mutations at Q288 are slow proliferating and exhibit a cell cycle checkpoint response (23). Each of the three mutations studied here (Y285F, Y285A and Q288A) have a different effect on dNTP pool balance, and spontaneous mutation rates. Here, we present an analysis of mutational specificity at the *CAN1* locus in these strains, and interpret the results in relation to the different dNTP pool imbalances in these strains and the models in Figure 1.

MATERIALS AND METHODS

Media and growth conditions

Cells were grown without selection in YPDA medium (1% yeast extract, 2% bacto-peptone, 2% dextrose, 250 mg/l adenine, 2% agar for plates). Can^r colonies were scored on synthetic complete medium containing 2% dextrose (SCD) lacking arginine and supplemented with 60 μg/ml canavanine. All growth was at 30°C.

Mutation rates

At least two independent isolates for each strain were used for both mutation rate analysis and mutation spectra assembly. Mutation rate protocol was previously described (23). Cultures were inoculated with single colonies and grown without selection in 5 ml YPDA to saturation (~2×10^8 cells/ml). Cells were washed with sterile double distilled water (ddH$_2$O) and resuspended in 1 ml of sterile ddH$_2$O. To calculate cell viability and mutation rates, 50–100 μl of the appropriate dilution was plated on YPDA and on SCD–Arg with canavaine, respectively. Colonies were counted after 2–4 days of growth. Mutation rates and associated 95% confidence intervals were determined by a modified method of the median (37,38).

CAN1 mutation spectra

A single canavanine-resistant colony from each culture was used to generate the spontaneous mutation spectrum to guarantee that each mutant resulted from an independent event. Mutant colonies were purified and genomic DNA was extracted. The sequence of the *CAN1* locus was amplified from the isolated DNA in two separate polymerase chain reactions (PCRs), and the resulting PCR products underwent automated DNA sequence analysis (Macrogen Inc. Seoul, Korea). The first half of the *CAN1* locus was amplified using primers PR1 5'-TCAGGGAATCCCTTTTTGCA and PR7 5'-TG AAATGTGAAGGCAGCGTT with the resulting PCR-amplified fragments sequenced by primers PR3 5'-CCAGTGGGCGCTCTTATA and PR8 5'-CGCCAG TGGAACTTTGTA. The latter half of the *CAN1* locus was PCR amplified using primers PR2 5'-GAAATGGCG TGGAAATGTGA and PR4 5'-TTACCGGCCCAGTTG GAT, this PCR product was the sequenced by PR5 5'-CA ACCATTATTTCTGCCG and PR9 5'-CCTGCAACAC CAGTGATA. Sequences were analyzed using Sequence Manager Software (DNA STAR Inc.).

Statistical analysis

Monte Carlo statistical analysis was performed to compare the distribution (number and location) of mutation events between spectra (39,40). Chi-square analysis was used to determine if a specific event occurred at a rate that is significantly different from the wild-type strain. Probability (*P*) values of <0.05 were considered significantly different.

RESULTS

dNTP pools and spontaneous mutation rates

We studied yeast strains harboring three different mutations in loop 2 of Rnr1, *rnr1-Y285F*, *rnr1-Y285A* and *rnr1-Q288A*. The *rnr1-Y285F* and *rnr1-Y285A* mutant strains progress through the cell cycle normally, whereas the strain containing the *rnr1-Q288A* mutation proliferates slowly and has a prolonged S-phase (23). The dNTP concentrations of the three mutant strains were measured by high performance liquid chromatography as reported previously (23). Compared to the dNTP levels in a wild-type strain, the *rnr1-Y285F* mutant strain has a 3-fold increase in the concentration of dTTP and dCTP, 1.8-fold increase in the concentration of dATP but no change in dGTP (Figure 2). The *rnr1-Y285A* mutant strain has dTTP, dCTP and dATP levels that are increased by 20-, 17- and 2-fold, respectively, but no change in dGTP (Figure 2). Finally, the *rnr1-Q288A* strain has dATP and dGTP levels increased by 6.6- and 16-fold, respectively, no significant change in the concentration of dTTP, and a 12-fold decrease in dCTP compared to the level in the wild-type strain (Figure 2). The low dCTP concentration could cause a stall in replication fork progression, explaining the slow S-phase progression and S-phase checkpoint activation in the *rnr1-Q288A* strain (23). In addition to
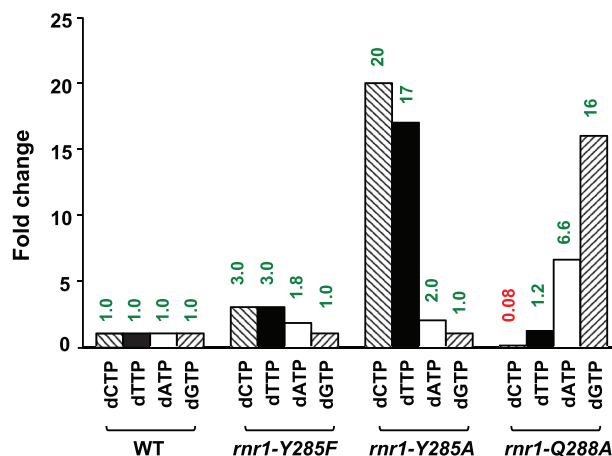

Figure 2. Graphical depiction of the fold change in the dNTP pool concentrations for the wild-type, *rnr1-Y285F*, *rnr1-Y285A*, and *rnr1-Q288A* strains. Numbers above the bars indicate fold-increase (green) or fold-decrease (red) of the dNTP concentration relative to wild-type. The actual dNTP pools in the wild-type strain were 41 pmol dCTP, 81 pmol dTTP, 35 pmol dATP and 15 pmol dGTP per 10^8 cells.

having alterations in dNTP pools, the three *rnr1* mutant strains have different spontaneous rates of mutation. The mutation rates were measured at the *CAN1* locus, using an assay that detects mutations that yield a non-functional protein, thereby allowing cells to grow on media containing canavanine. The mutation rate in the wild-type strain was 4×10^{-7}. The rates in the *rnr1-Y285F*, *rnr1-Y285A* and *rnr1-Q288A* strains were higher, at 11×10^{-7}, 57×10^{-7} and 17×10^{-7}, respectively (23).

Mutational specificity

The location and identity of the sequence changes in the open reading frame that were responsible for resistance were determined by the isolation of independent canavanine-resistant colonies, preparation of the colonies genomic DNA and sequencing of the *CAN1* locus (Figure 3A). The rates of specific types of mutations were then calculated by multiplying the percentage of that event by the total mutation rate. The sequence changes associated with the 93 mutants sequenced of the wild-type strain (Table 1) were distributed throughout the open reading frame (Figure 3B). Sixty-five of the mutations were single base substitutions, 11 were single base indels and the remaining mutations were larger deletions and complex events involving multiple base pairs. This specificity is similar to wild-type *CAN1* mutation spectra reported by others (41,42).

For the *rnr1-Y285F* strain, 93 mutants were sequenced (Table 1). The spectrum (Figure 3C) was largely comprised of base substitutions (78 of 93), such that the substitution rate was 3-fold higher than in the wild-type strain (Table 1, 9.2×10^{-7} versus 2.9×10^{-7}). Only 17% of the mutations in the *rnr1-Y285F* spectrum share a location in common with those in the wild-type spectrum. This difference is highly statistically significant ($P < 0.0001$).

The spectrum in the *rnr1-Y285A* strain, which has elevated dTTP and dCTP and a higher mutation rate, is strikingly different. At 18 locations in *CAN1* (red and blue symbols in Figure 3D), mutation rates were 20- to >300-fold higher than in the wild-type strain. Moreover, the spectrum is dominated by indels (101/173), yielding an average increase in the indel rate of 66-fold compared to the wild-type strain (Table 1, 0.5×10^{-7} versus 33×10^{-7}). Additionally, 97% of the indel mutations (98 of 101, Table 1) are single base pair deletions (triangles in Figure 3D), most of which are in one of three hotspots between base pairs 780–880 (Figure 3D). Seventy-two base substitutions were also observed, corresponding to an 8-fold increase in substitution rate relative to the wild-type strain (Table 1, 24×10^{-7} versus 2.9×10^{-7}). Interestingly, >80% of the base substitutions were transversions (Table 1), the majority of which (45 of 59) occurred at G•C base pairs.

The *rnr1-Q288A* strain has a mutation spectrum (Figure 3E) that differs significantly ($P < 0.0001$) from the three other spectra by Monte Carlo analysis. In this strain, 124 of 169 mutants were single base substitutions, 65% of which were transitions (Table 1). The distribution of substitutions (circles and squares in Figure 3E) was

non-random, such that substitution rates at five different locations in *CAN1* were from 10- to 50-fold higher than the wild-type strain. In addition, 41 of the *rnr1-Q288A* mutants had indel mutations corresponding to an 8-fold increase in the overall indel error rate (Table 1, 4.1×10^{-7} versus 0.5×10^{-7}). Similar to the base substitution mutations, the indels cluster into five mutation hotspots with mutation rates that are 10-fold higher than in the wild-type strain (triangles in Figure 3E).

Mutation hotspots

Table 2 list the nucleotide positions within the *CAN1* gene in the *rnr1-Y285A* and *rnr1-Q288A* strains where single base substitution and deletion rates are at least 10-fold higher than the rate in the wild-type strain. The events listed in the tables correspond to the red and blue hotspots displayed in Figure 3. The red hotspots are mutations that are predicted to have occurred when the non-coding strand is the template for replication, and the blue symbols represent mutations that are predicted to have occurred when the coding strand is the template for replication (Figure 3A). Also listed in Tables 2 and 3 are the number of occurrences of each event at the hotspot, the corresponding mutation rates and the fold-increase in rate over the mutation rate for that event in the wild-type strain. The last column in the tables shows the sequences of both DNA strands at the hotspots, with the presumptive error in red and the adjacent correct nucleotides that are in excess in green. The green letters in bold print correspond to correct bases with dNTP concentrations at least 5-fold greater than the dNTP concentration measured in the wild-type strain. The green letters in non-bold print represent dNTPs present at levels that are 2- to 5-fold greater than the wild-type levels. The DNA sequences are displayed in this manner to facilitate discussion of possible mutational mechanisms (see later).

DISCUSSION

The major goal of this study was to determine the extent to which the ideas outlined in Figure 1 can explain the specificity of mutagenesis observed *in vivo* when dNTP pools are selectively perturbed. Despite the fact that the *rnr1-Y285A* and *rnr1-Q288A* strains harbor very different dNTP pool imbalances and do not have a single mutational hotspot in common (red and blue symbols in Figure 3D/E), all 28 hotspots in *CAN1* can be explained by dNTP pool induced increases in three processes that determine DNA replication fidelity: dNTP MI, DNA strand MA and mismatch extension at the expense of proofreading.

Deletion hotspots

The highest mutation rate for any hotspot (12×10^{-7}, Table 2) is for the loss of a G•C base pair at positions 857–859. This hotspot was observed in the *rnr1-Y285A* strain, where the dNTP concentrations are lowest for dGTP and highest for dCTP and dTTP. The deletion is consistent with two models depicted in Figure 4.
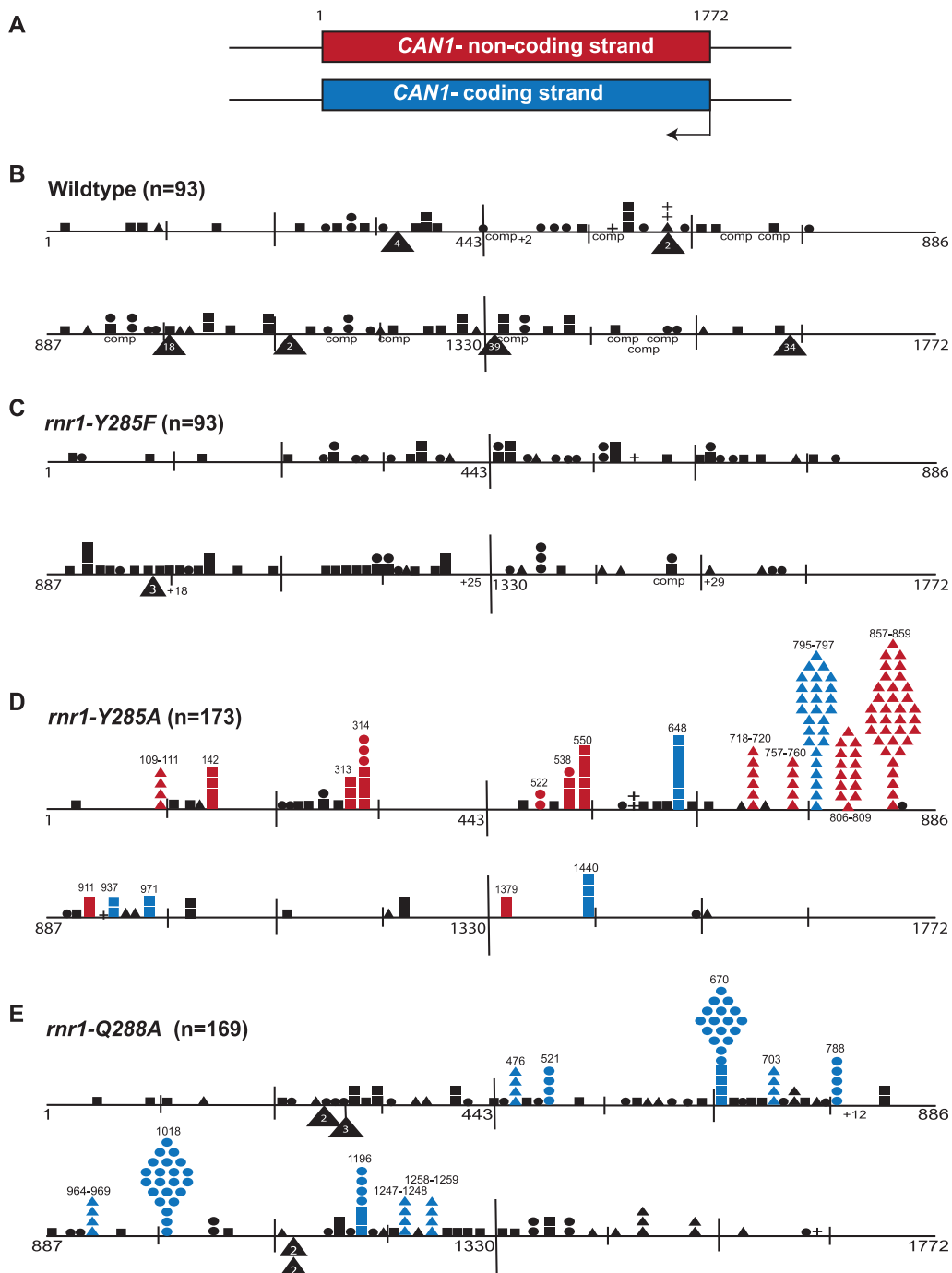
Figure 3. *CAN1* strand diagram (**A**) and mutational spectra of the wild-type (**B**), *rnr1-Y285F* (**C**), *rnr1-Y285A* (**D**) and the *rnr1-Q288A* (**E**) strains with 'n' equaling the number of events sequenced. The horizontal black line represents the *CAN1* coding sequence with the top line representing base pairs 1–886 and the bottom line representing base pairs 887–1772, the space between each tick mark represents ∼100 bp. Symbols above the line represent single base pair mutation events, filled circles are transitions, filled squares are transversions, filled triangles are deletions and plus signs are insertions. The symbols below the line indicate events that affect multiple nucleotides, primarily deletion greater than one base pair (black triangles), insertions (numbers preceded by the plus sign) and complex mutations (comp), which are multiple mutations within a 10 nucleotides. The red events mark hotspots where the mutation rate is at least 10-fold higher than in the wild-type spectrum and occurred on the non-coding strand of the *CAN1* gene. The blue events mark hotspots where the mutation rate is at least 10-fold higher than in the wild-type spectrum and occurred on the coding strand of the *CAN1* gene. The numbers above the mutational hotspots indicate the nucleotide position of the mutation within the *CAN1* gene.

One (Figure 4A, left branch) involves increased MA when replicating a CCC template, followed by RE of the mis-aligned intermediate via IN of 10 consecutive correct dTTPs and dCTPs, which are in excess. In fact, all six of the deletion hotspots in the *rnr1-Y285A* strain involve template cytosine run with adenine as a 5′neighbor (Table 2). Therefore, the high dGTP:dTTP ratio in the *rnr1-Y285A* strain could promote deletions via MI of

Table 1. Mutation rates of specific mutation events

	Mutation rates × 10^{-7}			
	Wild-type	rnr1-Y285F	rnr1-Y285A	rnr1-Q288A
Totals[a]	4.2[a] (93)	11[a] (93)	57[a] (173)	17[a] (169)
Base substitutions	2.9 (65)	9.2 (78)	24 (72)	12.4 (124)
Transitions	1.1 (24)	3.5 (30)	4.3 (13)	8.0 (80)
Transversions	1.9 (41)	5.7 (48)	20 (59)	4.4 (44)
Indels	0.5 (11)	1.2 (10)	33 (101)	4.1 (40)
Deletions	0.4 (8)	1.1 (9)	32 (98)	3.9 (39)
Other	0.8 (17)	0.6 (5)	<0.3[b]	0.5 (5)

(Number) = the number of events of that type observed.
[a]Data previously published (23).
[b]No event observed, rate is based on one event.

dTTP opposite template C, followed by PR (second model, Figure 4A, right branch). It is also possible that an MA within the polymerase active site (6) may be stabilized by excess dTTP, in a model called dNTP stabilized MA (43,44). These models are not mutually exclusive, and each of them is consistent with the deletions observed in these sequence contexts resulting from the *rnr1-Y285A* induced dNTP pool imbalances.

The five deletion hotspots in the *rnr1-Q288A* strain are at different locations than the hotspots observed in the *rnr1-Y285A* strain (Figure 3 and Table 2). Two hotspots in the *rnr1-Q288A* strain (at 1247–1248 and at 1258–1259) involve deleting a G•C base pair from small G•C runs, and a third (964–969) involves deleting an A•T base pair from a 6 bp A•T homopolymer run, one of the longest mononucleotide runs within the *CAN1*

Table 2. Strong dNTP bias-dependent single base deletion hotspots

Position	Mutation[a]	No of occurrences	Mutation rate (x10^{-7})	Fold increase over wild-type	Predicted intermediate
Y285A[b]: 17 × dTTP, 20 × dCTP, 2 × dATP, 1 × dGTP					
857–859	ΔG	35	12.0	≥300	5`TT**GGTTTCCTCTTT** AACCAAAGGAGAAACTA C
795–797	ΔC	27	8.9	≥200	C 5`TCCGTTATTGGAGAAACCAG **CAATAACCTCTTTGG**TC
718–720	ΔG	6	2.0	50	5`TC**GGTTTCTAATATACT** AGCCAAAGATTATATGACAA C
109–111	ΔG	4	1.3	≥30	5`GT**GGTCAATACCATT** CACCAGTTATGGTAACTT C
806–809	ΔG	14	4.6	≥100	5`CT**GGGTCCA** GACCCAGGTCCA C
757–760	ΔG	5	1.7	≥40	5`CT**GGGTTACC** GACCCAATGGCCG C
Q288A[b]: 1 × dTTP, 0.08 × dCTP, 7 × dATP, 16 × dGTP					
1247–1248	ΔG	4	0.4	≥10	G 5`CTGTCAAGAC **AG**TT**C**TG
1258–1259	ΔG	4	0.4	≥10	G 5`AGGACCACCAAAGTG **TGGTGG**TTT**C**AC
964–969	ΔA	4	0.4	≥10	A 5`GAGCCATCAAAAAGT **GGTAGTTTTT**CA
476	ΔG	4	0.4	≥10	G 5`CAGTTTTCTCACAAAAT **AAAAGAG**TG**TTTT**A
703	ΔG	4	0.4	≥10	G 5`TCGCTTCCATCAAATT **GAAGGTAG**TTTAA

The predicted mutation is noted red.
The characters in green represent nucleotides that are extended after the mutation from dNTPs present at higher than wild-type concentrations.
[a]The mutation observed on the coding or top strand of the *CAN1* sequence displayed.
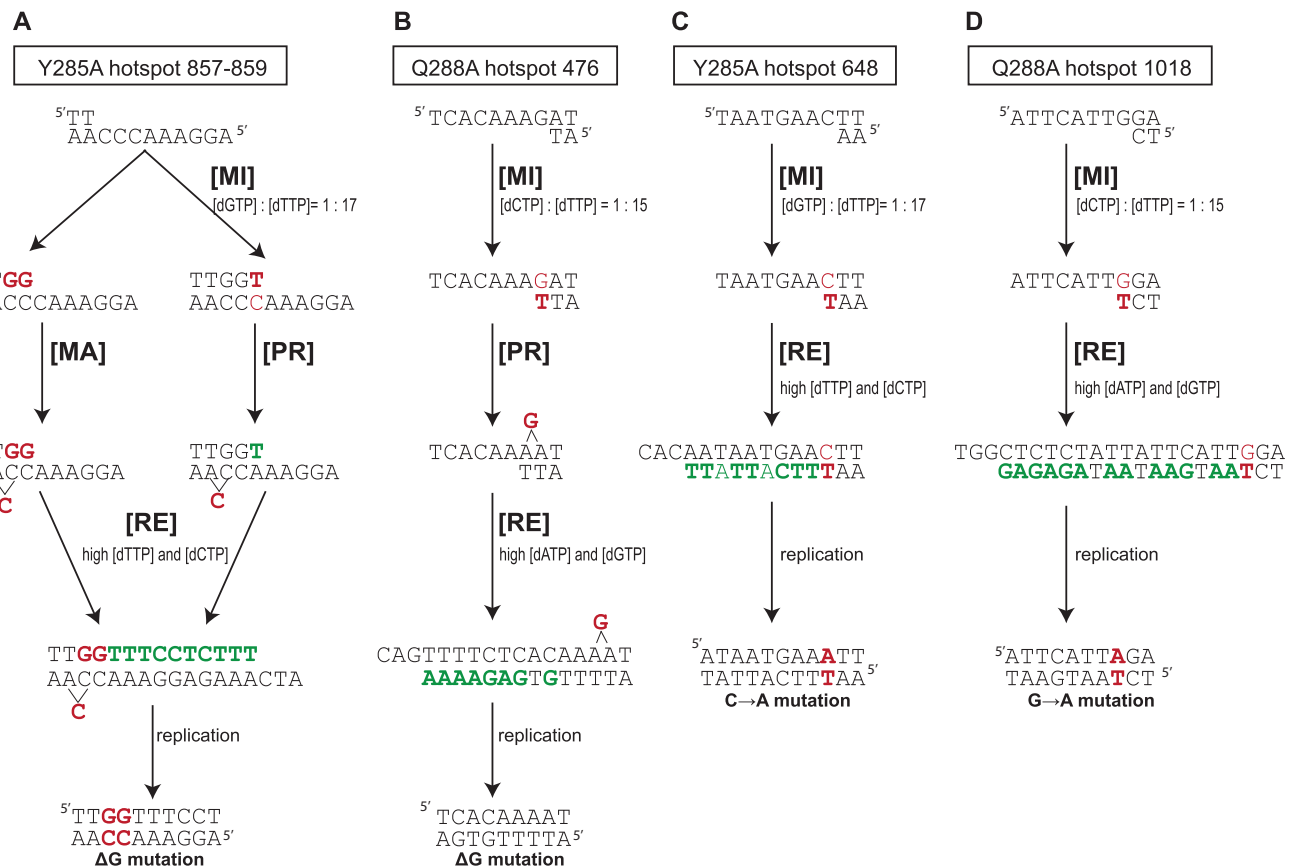[b]dNTP pool concentrations were published previously (23).

Figure 4. Examples of predicted mutational mechanism associated with observed mutation hotspots in *rnr1-Y285A* and *rnr1-Q288A*. Red characters represent the mutational event and green bases represent bases where the dNTP is at an excessively high concentration. MI: misinsertion; MA: misalignment; PR: primer relocation; RE: rapid extension. The numbers listed below the (MI) labels in **A–D** refer to the ratios of the correct nucleotide compared to the incorrect/misinserted nucleotide relative to wild type.

locus. These hotspots have explanations similar to those in the *rnr1-Y285A* strain (see last column in Table 2), but reflect the different dNTP pool imbalance in the *rnr1-Q288A* strain. Note that in all three cases, one of the next correct nucleotides, dTTP, is not in large excess. This might result in less efficient extension and correspondingly more proofreading, perhaps contributing to the lower rate of mutation at these sites as compared to the deletion hotspots in the *rnr1-Y285A* strain.

The two hotspots in the *rnr1-Q288A* strain that occur at nucleotides 476 and 703 involve deleting a non-iterated G•C base pair (Table 2). This is particularly informative, in that non-iterated bases are not usually seen as hotspots for deletions. Commonly, strand MAs at non-iterated nucleotides do not generate intermediates that can be stabilized by the correct base pairing, which is possible at repetitive sequences [reviewed in (45)]. Because these two non-iterated sites accumulate multiple mutations in a strain with imbalanced dNTP pools, we suggest that the initiating event for these deletions is MI of dTTP opposite template G (e.g. site 476, Figure 4B), followed by PR to allow T to pair with its 5′template neighbor, an adenine. In both cases, the next correct nucleotides are in excess to promote extension of the MA.

Base substitution hotspots

Despite being completely different in the *rnr1-Y285A* strain as compared to the *rnr1-Q288A* strain (Table 3), all 18 base substitution hotspots can be rationalized by dNTP pools that increase dNTP MI and then also increase subsequent mismatch extension. For example, the C to A substitution hotspot at position 648 (Figure 4C) in the *rnr1-Y285A* strain would result from MI of dTTP opposite template C due to the high ratio of dTTP compared to dGTP, followed by the RE of approximately nine nucleotides from the mismatch, which is promoted by the high concentrations of dTTP and dCTP. Similarly, the G to A substitution hotspot at position 1018 in the *rnr1-Q288A* strain (Figure 4D) would result from MI of dTTP opposite template G due to the high ratio of dTTP compared to dCTP, followed by rapid IN of the next 15 correct nucleotides promoted by the excessively high concentrations of dATP and dGTP.

A non-exclusive alternative can be considered for two of the eight substitution hotspots in the *rnr1-Y285A* strain. At base pairs 314(a) and 1440 (Table 3), a G to T substitution occurs at the 5′-G in a run that in each case is flanked by a T. At these sites, the rightmost pathway in Figure 1, involving MA, correct IN, RA and mismatch extension, could also contribute to formation of these substitutions.

Table 3. Strong dNTP bias-dependent base substitution hotspots

Position	Mutation[a]	No of occurrences	Mutation rate (x10^{-7})	Fold increase over wild-type	Predicted intermediate
Y285A[b]: 17 × dTTP, 20 × dCTP, 2 × dATP, 1 × dGTP					
648	C → A	6	2.0	≥50	5`CACAATAATGAACTT TTATTACTTTTAA
550	G → T	6	2.0	50	5`TGTAACTTA ACCTTGAATCAC
1440	C → A	4	1.3	≥30	5`AGCTTTGAAATACCG AAACTTTATTGC
142	G → T	4	1.3	≥30	5`AATAATT TTCTTAACAT
314 (a)	G → T	4	1.3	30	5`AGTTCTTTTCATT TCCAGAAAAGTAACCA
314 (b)	G → A	3	1.0	20	5`AGATCTTTTCATT TCCAGAAAAGTAACCA
313	G → T	3	1.0	≥20	5`CATGTCTTTTCATT GTCCAGAAAAGTAACCA
538	A → C	3	1.0	20	5`TCCCTTTT TGCGAAAACGG
522	G → A	2	0.7	≥15	5`TGATTTTCTT ACCAAAAGAACCC
911	G → T	2	0.7	≥15	5`TGTTATCACT ACCATAGTGACGA
937	C → A	2	0.7	≥15	5`TGCAAACCCC TTTGTGG
971	T → A	2	0.7	≥15	5`ATCAAAAAAGATG TTTTTTCAAC
1379	G → T	2	0.7	≥15	5`AGTCTTTTTT TCCGAAAAAACGT
Q288A[b]: 1 × dTTP, 0.08 × dCTP, 7 × dATP, 16 × dGTP					
1018	G → A	22	2.2	≥50	5`TGGCTCTCTATTATTCATTGGA GAGAGATAATAAGTAATCT
670 (a)	G → A	17	1.7	≥40	5`CTGTCAAATATTACGGT AGTTTATAATGTCA
670 (b)	G → T	4	0.4	10	5`CTGTCAAATATTACGGT AGTTTATAATGACA
788	G → A	5	0.5	≥10	5`CCGTTATTGGA AATAATCT
521	G → A	4	0.4	10	5`ATGTATTGGT ATAATCA
1196	G → A	4	0.4	≥10	5`TGGTTCCCGTA AAGGGTAT

The predicted mutation is noted red.
The characters in green represent nucleotides that are extended after the mutation from dNTPs present at higher than wild-type concentrations.
[a]The mutation observed on the coding or top strand of the *CAN1* sequence displayed.
[b]dNTP pool concentrations were published previously (23).

Competition by mass action for correct versus incorrect dNTP insertion at the polymerase active site also rationalizes a more general difference between the two *rnr1* mutant strains involving base substitutions at G–C base pairs (Table 1). The *rnr1-Y285A* mutation enhances transversions to a greater extent than it enhances transitions, especially at G•C base pairs (Table 1). This is anticipated by the unusually high relative ratio of dTTP to dGTP (17:1) as compared to the more normal relative ratio of dATP to dGTP (2:1)

(Figure 2). In comparison, the *rnr1-Q288A* mutation enhances G to A transitions to a slightly greater extent than it enhances G to T transversions (Table 1). The concentrations of both dTTP and dATP are significantly higher than the concentration of dCTP. The relative ratios of dTTP to dCTP and of dATP to dCTP are 15:1 and 83:1, respectively (Figure 2). Interestingly, even though dTTP is not as abundant as dATP it is the favored base substitution in the *rnr1-Q288A* strain.

Strand bias in mutagenesis induced by dNTP pool imbalances

As mentioned earlier, the six deletion hotspots in the *rnr1-Y285A* strain were all runs of G•C base pairs. There are 28 runs of three or more G•C base pairs in the *CAN1* open reading frame, 14 with guanine and 14 with cytosine in the coding strand. Interestingly, five of the six hotspots involved coding strand guanine runs (Table 2).

This is a statistically significant difference by chi-square analysis ($P = 0.0005$), indicating a strand bias in formation of single base deletions resulting from imbalanced dNTP pools. Further evidence for a strand bias comes from comparing the hotspots depicted in red versus blue colors in Figure 3. In the *rnr1-Y285A* spectrum, 13 of the 18 hotspots are predicted to have resulted from replication of the non-coding strand of the *CAN1* gene (red), and five are predicted to have resulted from replication of the *CAN1* coding strand (blue). In contrast, all 10 hotspots in the *rnr1-Q288A* strain are predicted to result from replication of the coding strand of the *CAN1* gene. Additionally, the mutation hotspots within the *CAN1* locus of a strain harboring and over-expressing a plasmid copy of *rnr1-Q288A* were also predicted to exclusively occur on the coding strand (data not shown). This difference between the *rnr1-Y285A* and *rnr1-Q288A* strains is highly significant ($P = 0.0008$).

Does the checkpoint response prevent leading strand mutagenesis?

This putative asymmetric distribution of mutations on the coding strand in the *rnr1-Q288A* strain but not in the *rnr1-Y285A* strain suggests that mutagenesis can be differentially modulated during leading strand and lagging strand replication, depending on the nature of the pool imbalance. How might this occur? Previous analysis of early firing replication origins on the left arm of chromosome five of *S. cerevisiae* has shown that replication of the *CAN1* gene originates from ARS507 and travels through *CAN1* towards the telomere (46–48). This predicts that the non-coding strand should be the template for leading strand replication, and that the coding strand should be the template for lagging strand replication. Current evidence suggests that the leading strand template may primarily be replicated by Pol ε (49), whereas the lagging strand template may primarily be replicated by Pol δ (50). These facts are intriguing, given that (i) the *rnr1-Y285A* strain proliferates normally but the *rnr1-Q288A* strain proliferates slowly, has a defect in S-phase progression and elicits a checkpoint response (23) and (ii) Pol ε, but not Pol δ, is involved in the S-phase checkpoint response (51,52). Thus, the surprising absence of putative non-coding (i.e. leading) strand hotspots in the *rnr1-Q288A* strain despite the large dNTP pool imbalance may be related to Pol ε's combined roles in leading strand replication and in the S-phase checkpoint response. In other words, as Pol ε attempts leading strand replication using too little dCTP and excess dATP and dGTP, certain mismatches that are known to be particularly difficult to extend [e.g. G-dAMP and G-dGMP, (53)]

may be prevented from yielding mutations via Pol ε's checkpoint function. Conceptually, this is similar to the idea that checkpoints initiated by DNA lesions stall replication to provide more time for DNA repair. In the present case, the checkpoint response may provide more time for error correction from proofreading by Pol ε, whose 3′-exonuclease is processive and highly active (54,55). A checkpoint might even allow more time for mismatch repair to correct leading strand replication errors, especially if replication and mismatch repair are coupled (56). Because there are still many coding (i.e. putative lagging) strand mutational hotspots in the *CAN1* spectrum in the *rnr1-Y285A* strain, a checkpoint mechanism to reduce mutagenesis might not apply to lagging strand replication errors made by Pol δ, a polymerase with no reported role in the S-phase checkpoint response (Figure 5). It should also be noted that an activated S-phase checkpoint inhibits replication origin firing (57–59), which could be relevant to the strand biases observed here. Alternatively, it is also possible that differences in the distribution of mutations on the two strands might be related to differences in the efficiency with which pols α/δ versus pol ε extend mismatches driven by high dTTP/dCTP versus those that are driven by high dATP/dGTP. In the future, we plan to further examine this unexpected strand specificity, using *rnr1* mutants in combination with mutator alleles of DNA polymerases δ and ε, in a system previously used to study leading and lagging strand replication fidelity in yeast (49,50).

Additional implications

The *rnr1-Y285A* strain has a higher dNTP pool imbalance and a higher mutation rate than does the *rnr1-Y285F* mutant (23). This correlation, and the fact that the observed mutational specificity can be rationalized by the models in Figure 1, implies that the elevated mutation rates for the *rnr1* mutant strains are indeed the result of reduced DNA replication fidelity *in vivo*. It then follows that the dNTP concentrations that were measured here in extracts reflect the relative biologically relevant ratios of dNTPs that are available to a replication fork *in vivo*. This suggests that selective compartmentalization
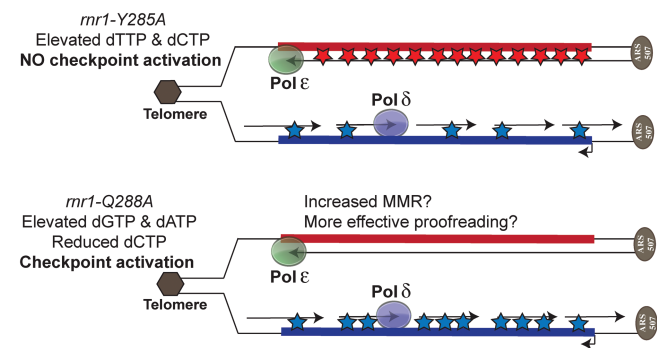

Figure 5. Cartoon depiction of the hypothesized replication fidelity bias mediated by Pol ε on the leading template when the S-phase checkpoint is activated. Blue and red stars depict hotspot events.

or channeling of dNTPs is not occurring *in vivo*, at least in budding yeast (1,60). This validates the continued use of HPLC analysis of cell extracts to measure biologically relevant dNTP pools.

Because dNTP pool imbalances reduce genome stability to different extents and with specificities that are highly dependent on the nature and degree of the imbalance, it follows that different dNTP pool imbalances may put specific genes at increased risk of inactivation by substitution and indel mutations. In this study, this risk is apparent despite the fact that the two major replication error correction mechanisms, proofreading and DNA mismatch repair, are genetically intact. Thus, it is possible that the mutagenesis observed here is merely the 'tip of the iceberg'. Much of the mutagenic potential of dNTP pool imbalances may be offset by error correction, which could explain why some sites exist in *CAN1* where we might expect to see mutations were not hotspots. As one example, no deletions were observed at a run of three G•C base pairs at positions 387–389, even though the sequence context (5′-GGGTTC) is remarkably similar to that of the deletion hotspot at positions 857–859 (5′-GGG TTTC) observed in the *rnr1-Y285A* strain. The mutational specificity observed here (Tables 2 and 3) indicates that at least one of the two well-known error correction mechanisms, proofreading, is being suppressed via rapid mismatch extension due to high concentrations of the next correct nucleotides to be incorporated after a mismatch is generated. However, we were surprised to observe such a high proportion of single base deletion mutations in the *rnr1-Y285A* strain, because the mismatch repair machinery normally corrects single base indel mismatches very efficiently. In fact, indels are rarely observed in *CAN1* spectrum of mutator strains (41,61,62), unless mismatch repair is inactivated (41). The deletion and substitution mutations observed here obviously escaped mismatch repair, perhaps because the dNTP pool imbalance result in so many replication errors that mismatch repair is partially saturated (63,64), or alternatively, because the hotspots occur in sequence contexts where mismatch repair is intrinsically less efficient (65).

ACKNOWLEDGEMENTS

FUNDING

REFERENCES

1. Reichard,P. (1988) Interactions between deoxyribonucleotide and DNA synthesis. *Annu. Rev. Biochem.*, **57**, 349–374.
2. Kunz,B.A., Kohalmi,S.E., Kunkel,T.A., Mathews,C.K., McIntosh,E.M. and Reidy,J.A. (1994) International Commission for Protection Against Environmental Mutagens and Carcinogens. Deoxyribonucleoside triphosphate levels: a critical factor in the maintenance of genetic stability. *Mutat. Res.*, **318**, 1–64.
3. Kunkel,T.A. (1992) DNA replication fidelity. *J. Biol. Chem.*, **267**, 18251–18254.
4. Bebenek,K., Roberts,J.D. and Kunkel,T.A. (1992) The effects of dNTP pool imbalances on frameshift fidelity during DNA replication. *J. Biol. Chem.*, **267**, 3589–3596.
5. Bebenek,K., Abbotts,J., Wilson,S.H. and Kunkel,T.A. (1993) Error-prone polymerization by HIV-1 reverse transcriptase. Contribution of template-primer misalignment, miscoding, and termination probability to mutational hot spots. *J. Biol. Chem.*, **268**, 10324–10334.
6. Kunkel,T.A. (1986) Frameshift mutagenesis by eucaryotic DNA polymerases in vitro. *J. Biol. Chem.*, **261**, 13581–13587.
7. Kunkel,T.A. and Soni,A. (1988) Mutagenesis by transient misalignment. *J. Biol. Chem.*, **263**, 14784–14789.
8. Roberts,J.D. and Kunkel,T.A. (1988) Fidelity of a human cell DNA replication complex. *Proc. Natl Acad. Sci. USA.*, **85**, 7064–7068.
9. Kunkel,T.A. (1985) The mutational specificity of DNA polymerases-alpha and -gamma during in vitro DNA synthesis. *J. Biol. Chem.*, **260**, 12866–12874.
10. Kunkel,T.A. (1985) The mutational specificity of DNA polymerase-beta during in vitro DNA synthesis. Production of frameshift, base substitution, and deletion mutations. *J. Biol. Chem.*, **260**, 5787–5796.
11. Phear,G. and Meuth,M. (1989) The genetic consequences of DNA precursor pool imbalance: sequence analysis of mutations induced by excess thymidine at the hamster aprt locus. *Mutat. Res.*, **214**, 201–206.
12. Phear,G. and Meuth,M. (1989) A novel pathway for transversion mutation induced by dCTP misincorporation in a mutator strain of CHO cells. *Mol. Cell. Biol.*, **9**, 1810–1812.
13. Phear,G., Nalbantoglu,J. and Meuth,M. (1987) Next-nucleotide effects in mutations driven by DNA precursor pool imbalances at the aprt locus of Chinese hamster ovary cells. *Proc. Natl Acad. Sci. USA.*, **84**, 4450–4454.
14. Sargent,R.G. and Mathews,C.K. (1987) Imbalanced deoxyribonucleoside triphosphate pools and spontaneous mutation rates determined during dCMP deaminase-defective bacteriophage T4 infections. *J. Biol. Chem.*, **262**, 5546–5553.
15. Glickman,B.W., Allen,F.L. and Horsfall,M.J. (1988) Mutational specificity of thymine deprivation-induced mutation in the lacI gene of *Escherichia coli*. *Mutat. Res.*, **200**, 177–182.
16. Mattano,S.S., Palella,T.D. and Mitchell,B.S. (1990) Mutations induced at the hypoxanthine–guanine phosphoribosyltransferase locus of human T-lymphoblasts by perturbations of purine deoxyribonucleoside triphosphate pools. *Cancer Res.*, **50**, 4566–4571.
17. Ji,J. and Mathews,C.K. (1993) A forward mutation assay in phage T4: application to gene 42 mutator mutations. *Mutat. Res.*, **294**, 247–254.
18. Ji,J.P. and Mathews,C.K. (1991) Analysis of mutagenesis induced by a thermolabile T4 phage deoxycytidylate hydroxymethylase suggests localized deoxyribonucleotide pool imbalance. *Mol. Gen. Genet.*, **226**, 257–264.
19. Kohalmi,S.E., Glattke,M., McIntosh,E.M. and Kunz,B.A. (1991) Mutational specificity of DNA precursor pool imbalances in yeast arising from deoxycytidylate deaminase deficiency or treatment with thymidylate. *J. Mol. Biol.*, **220**, 933–946.
20. Veigl,M.L., Schneiter,S., Mollis,S. and Sedwick,W.D. (1991) Specificities mediated by neighboring nucleotides appear to underlie mutation induced by antifolates in E coli. *Mutat. Res.*, **246**, 75–91.
21. Kohalmi,S.E. and Kunz,B.A. (1993) Mutational specificity of thymine nucleotide depletion in yeast. *Mutat. Res.*, **289**, 73–81.

22. Kresnak,M.T. and Davidson,R.L. (1992) Thymidine-induced mutations in mammalian cells: sequence specificity and implications for mutagenesis in vivo. *Proc. Natl Acad. Sci. USA.*, **89**, 2829–2833.

23. Kumar,D., Viberg,J., Nilsson,A.K. and Chabes,A. (2010) Highly mutagenic and severely imbalanced dNTP pools can escape detection by the S-phase checkpoint. *Nucleic Acids Res.*, **38**, 3975–3983.

24. Huang,M., Zhou,Z. and Elledge,S.J. (1998) The DNA replication and damage checkpoint pathways induce transcription by inhibition of the Crt1 repressor. *Cell*, **94**, 595–605.

25. Elledge,S.J. and Davis,R.W. (1990) Two genes differentially regulated in the cell cycle and by DNA-damaging agents encode alternative regulatory subunits of ribonucleotide reductase. *Genes Dev.*, **4**, 740–751.

26. Elledge,S.J. and Davis,R.W. (1987) Identification and isolation of the gene encoding the small subunit of ribonucleotide reductase from *Saccharomyces cerevisiae*: DNA damage-inducible gene required for mitotic viability. *Mol. Cell. Biol.*, **7**, 2783–2793.

27. Fernandez Sarabia,M.J., McInerny,C., Harris,P., Gordon,C. and Fantes,P. (1993) The cell cycle genes cdc22+ and suc22+ of the fission yeast Schizosaccharomyces pombe encode the large and small subunits of ribonucleotide reductase. *Mol. Gen. Genet.*, **238**, 241–251.

28. Zhao,X. and Rothstein,R. (2002) The Dun1 checkpoint kinase phosphorylates and regulates the ribonucleotide reductase inhibitor Sml1. *Proc. Natl. Acad Sci. USA.*, **99**, 3746–3751.

29. Yao,R., Zhang,Z., An,X., Bucci,B., Perlstein,D.L., Stubbe,J. and Huang,M. (2003) Subcellular localization of yeast ribonucleotide reductase regulated by the DNA replication and damage checkpoint pathways. *Proc. Natl Acad. Sci. USA*, **100**, 6628–6633.

30. Lee,Y.D., Wang,J., Stubbe,J. and Elledge,S.J. (2008) Dif1 is a DNA-damage-regulated facilitator of nuclear import for ribonucleotide reductase. *Mol. Cell.*, **32**, 70–80.

31. Wu,X. and Huang,M. (2008) Dif1 controls subcellular localization of ribonucleotide reductase by mediating nuclear import of the R2 subunit. *Mol. Cell. Biol.*, **28**, 7156–7167.

32. Thelander,L. and Reichard,P. (1979) Reduction of ribonucleotides. *Annu. Rev. Biochem.*, **48**, 133–158.

33. Nordlund,P. and Reichard,P. (2006) Ribonucleotide reductases. *Annu. Rev. Biochem.*, **75**, 681–706.

34. Eriksson,M., Uhlin,U., Ramaswamy,S., Ekberg,M., Regnstrom,K., Sjoberg,B.M. and Eklund,H. (1997) Binding of allosteric effectors to ribonucleotide reductase protein R1: reduction of active-site cysteines promotes substrate binding. *Structure*, **5**, 1077–1092.

35. Larsson,K.M., Jordan,A., Eliasson,R., Reichard,P., Logan,D.T. and Nordlund,P. (2004) Structural mechanism of allosteric substrate specificity regulation in a ribonucleotide reductase. *Nat. Struct. Mol. Biol.*, **11**, 1142–1149.

36. Xu,H., Faber,C., Uchiki,T., Fairman,J.W., Racca,J. and Dealwis,C. (2006) Structures of eukaryotic ribonucleotide reductase I provide insights into dNTP regulation. *Proc. Natl Acad. Sci. USA*, **103**, 4022–4027.

37. Lea,D.E. and Coulson,C.A. (1949) The distribution of the numbers of mutants in bacterial populations. *J. Genet.*, **49**, 264–285.

38. Drake,J.W. (1991) A constant rate of spontaneous mutation in DNA-based microbes. *Proc. Natl Acad. Sci. USA*, **88**, 7160–7164.

39. Adams,W.T. and Skopek,T.R. (1987) Statistical test for the comparison of samples from mutational spectra. *J. Mol. Biol.*, **194**, 391–396.

40. Cariello,N.F., Piegorsch,W.W., Adams,W.T. and Skopek,T.R. (1994) Computer program for the analysis of mutational spectra: application to p53 mutations. *Carcinogenesis*, **15**, 2281–2285.

41. Tishkoff,D.X., Filosi,N., Gaida,G.M. and Kolodner,R.D. (1997) A novel mutation avoidance mechanism dependent on S. cerevisiae RAD27 is distinct from DNA mismatch repair. *Cell*, **88**, 253–263.

42. Kokoska,R.J., Stefanovic,L., DeMai,J. and Petes,T.D. (2000) Increased rates of genomic deletions generated by mutations in the yeast gene encoding DNA polymerase delta or by decreases

43. Efrati,E., Tocco,G., Eritja,R., Wilson,S.H. and Goodman,M.F. (1997) Abasic translesion synthesis by DNA polymerase beta violates the 'A-rule'. Novel types of nucleotide incorporation by human DNA polymerase beta at an abasic lesion in different sequence contexts. *J. Biol. Chem.*, **272**, 2559–2569.

44. Hashim,M.F., Schnetz-Boutaud,N. and Marnett,L.J. (1997) Replication of template-primers containing propanodeoxyguanosine by DNA polymerase beta. Induction of base pair substitution and frameshift mutations by template slippage and deoxynucleoside triphosphate stabilization. *J. Biol. Chem.*, **272**, 20205–20212.

45. Garcia-Diaz,M. and Kunkel,T.A. (2006) Mechanism of a genetic glissando: structural biology of indel mutations. *Trends Biochem. Sci.*, **31**, 206–214.

46. Yabuki,N., Terashima,H. and Kitada,K. (2002) Mapping of early firing origins on a replication profile of budding yeast. *Genes Cells*, **7**, 781–789.

47. Raghuraman,M.K., Winzeler,E.A., Collingwood,D., Hunt,S., Wodicka,L., Conway,A., Lockhart,D.J., Davis,R.W., Brewer,B.J. and Fangman,W.L. (2001) Replication dynamics of the yeast genome. *Science*, **294**, 115–121.

48. Kim,H.M., Narayanan,V., Mieczkowski,P.A., Petes,T.D., Krasilnikova,M.M., Mirkin,S.M. and Lobachev,K.S. (2008) Chromosome fragility at GAA tracts in yeast depends on repeat orientation and requires mismatch repair. *EMBO J.*, **27**, 2896–2906.

49. Pursell,Z.F., Isoz,I., Lundstrom,E.B., Johansson,E. and Kunkel,T.A. (2007) Yeast DNA polymerase epsilon participates in leading-strand DNA replication. *Science*, **317**, 127–130.

50. Nick McElhinny,S.A., Gordenin,D.A., Stith,C.M., Burgers,P.M. and Kunkel,T.A. (2008) Division of labor at the eukaryotic replication fork. *Mol. Cell.*, **30**, 137–144.

51. Pursell,Z.F. and Kunkel,T.A. (2008) DNA polymerase epsilon: a polymerase of unusual size (and complexity). *Prog. Nucleic Acid Res. Mol. Biol.*, **82**, 101–145.

52. Navas,T.A., Zhou,Z. and Elledge,S.J. (1995) DNA polymerase epsilon links the DNA replication machinery to the S phase checkpoint. *Cell*, **80**, 29–39.

53. Huang,M.M., Arnheim,N. and Goodman,M.F. (1992) Extension of base mispairs by Taq DNA polymerase: implications for single nucleotide discrimination in PCR. *Nucleic Acids Res.*, **20**, 4567–4573.

54. Shcherbakova,P.V., Pavlov,Y.I., Chilkova,O., Rogozin,I.B., Johansson,E. and Kunkel,T.A. (2003) Unique error signature of the four-subunit yeast DNA polymerase epsilon. *J. Biol. Chem.*, **278**, 43770–43780.

55. Shcherbakova,P.V. and Pavlov,Y.I. (1996) $3'->5'$ exonucleases of DNA polymerases epsilon and delta correct base analog induced DNA replication errors on opposite DNA strands in *Saccharomyces cerevisiae*. *Genetics*, **142**, 717–726.

56. Umar,A., Buermeyer,A.B., Simon,J.A., Thomas,D.C., Clark,A.B., Liskay,R.M. and Kunkel,T.A. (1996) Requirement for PCNA in DNA mismatch repair at a step preceding DNA resynthesis. *Cell*, **87**, 65–73.

57. Pasero,P., Shimada,K. and Duncker,B.P. (2003) Multiple roles of replication forks in S phase checkpoints: sensors, effectors and targets. *Cell Cycle*, **2**, 568–572.

58. Shirahige,K., Hori,Y., Shiraishi,K., Yamashita,M., Takahashi,K., Obuse,C., Tsurimoto,T. and Yoshikawa,H. (1998) Regulation of DNA-replication origins during cell-cycle progression. *Nature*, **395**, 618–621.

59. Santocanale,C. and Diffley,J.F. (1998) A Mec1- and Rad53-dependent checkpoint controls late-firing origins of DNA replication. *Nature*, **395**, 615–618.

60. Mathews,C.K. (1993) Enzyme organization in DNA precursor biosynthesis. *Prog. Nucleic Acid Res. Mol. Biol.*, **44**, 167–203.

61. Huang,M.E., Rio,A.G., Galibert,M.D. and Galibert,F. (2002) Pol32, a subunit of *Saccharomyces cerevisiae* DNA polymerase delta, suppresses genomic deletions and is involved in the mutagenic bypass pathway. *Genetics*, **160**, 1409–1422.

62. Chen,C., Merrill,B.J., Lau,P.J., Holm,C. and Kolodner,R.D. (1999) *Saccharomyces cerevisiae* pol30 (proliferating cell nuclear

antigen) mutations impair replication fidelity and mismatch repair. *Mol. Cell. Biol.*, **19**, 7801–7815.

63. Schaaper,R.M. and Radman,M. (1989) The extreme mutator effect of *Escherichia coli* mutD5 results from saturation of mismatch repair by excessive DNA replication errors. *EMBO J.*, **8**, 3511–3516.

64. Fijalkowska,I.J. and Schaaper,R.M. (1996) Mutants in the Exo I motif of *Escherichia coli* dnaQ: defective proofreading and inviability due to error catastrophe. *Proc. Natl Acad. Sci. USA*, **93**, 2856–2861.

65. Nick McElhinny,S.A., Watts,B.E., Kumar,D., Watt,D.L., Lundstrom,E.B., Burgers,P.M., Johansson,E., Chabes,A. and Kunkel,T.A. Abundant ribonucleotide incorporation into DNA by yeast replicative polymerases. *Proc. Natl Acad. Sci. USA*, **107**, 4949–4954.